Lattice QCD Benchmark of Proton Helicity and Flavor-Dependent Unpolarized Transverse Momentum-Dependent Parton Distribution Functions at Physical Quark Masses

Dennis Bollweg,[1] Xiang Gao,[2,*] Swagato Mukherjee,[2] and Yong Zhao[3]
[1]Computing and Data Sciences Directorate, Brookhaven National Laboratory, Upton, New York 11973, USA
[2]Physics Department, Brookhaven National Laboratory, Upton, New York 11973, USA
[3]Physics Division, Argonne National Laboratory, Lemont, Illinois 60439, USA

(Received 23 June 2025; revised 24 September 2025; accepted 20 October 2025; published 12 November 2025)

We present the first lattice QCD calculations of the isovector helicity transverse momentum-dependent parton distribution function (TMDPDF) and the flavor-dependent unpolarized TMDPDFs for up and down quarks in the proton. Our computations utilize domain-wall fermion discretization with physical quark masses. Employing Coulomb-gauge-fixed quark correlation functions within the large-momentum effective theory framework, we access nonperturbative transverse quark separations b_T up to approximately 1 fm, corresponding to transverse momenta as low as 200 MeV. Based on the quasi-TMD factorization theorem, we construct renormalization-group–invariant ratios that are equal to the corresponding light-cone TMDPDF ratios. At moderate x, our results reveal that the isovector helicity and unpolarized TMDPDFs exhibit nearly identical transverse structure up to a normalization factor, and the unpolarized distributions display only mild flavor dependence. These findings not only support key trends observed in recent global analyses but also provide robust, nonperturbative constraints that can distinguish between different parameterizations. This Letter establishes a first-principles benchmark for TMDPDFs, offering valuable input for ongoing and future experimental efforts to map the proton's three-dimensional structure.

DOI: 10.1103/tb2w-3tks

Introduction—Protons, as the stable constituents of atomic nuclei, form the basis of visible matter. Understanding their internal structure and dynamics from first principles of quantum chromodynamics (QCD), the theory of strong interactions, is a central goal of modern theoretical and experimental physics. This requires unraveling how the proton's spin emerges from its quark and gluon constituents. While collinear parton distribution functions (PDFs) provide information on longitudinal momentum structure, a complete picture of proton spin demands access to its full three-dimensional momentum structure. Transverse momentum-dependent PDFs (TMDPDFs) generalize PDFs by incorporating dependence on both the longitudinal momentum fraction x and transverse momentum k_T. This makes TMDPDFs central to the scientific objectives of experiments at facilities such as Jefferson Lab [1,2], the Large Hadron Collider (LHC) [3,4], and the upcoming Electron-Ion Collider (EIC) [5–8], which will explore the proton's spin structure with unprecedented precision.

Among leading-twist TMDPDFs, the helicity distribution encodes the density of longitudinally polarized quarks in a longitudinally polarized proton, while retaining k_T dependence. It plays a key role in resolving spin and orbital contributions of partons to the proton's total spin. The unpolarized TMDPDF, in contrast, describes intrinsic k_T distributions irrespective of spin and serves as a baseline for spin-dependent observables. The flavor dependence of TMDPDFs is sensitive to valence-sea structure and isospin symmetry breaking, and is essential for interpreting transverse spin asymmetries and constraining global fits.

Phenomenological parametrizations of the unpolarized TMDPDF from global fits to semi-inclusive deep inelastic scattering and Drell-Yan data have made substantial progress in the past four decades [9–29], including recent studies of its flavor dependence [30,31]. This approach is limited by sparse data in the kinematic region sensitive to nonperturbative physics and rely on model-dependent assumptions at low k_T, where there are still tensions among different groups. In contrast, global fits of the proton helicity TMDPDF have only become available very recently [32,33], but the results from the two groups show noticeable inconsistencies.

Lattice QCD is a first-principles approach that can calculate the spin- and flavor-resolved hadron structure in the nonperturbative regime. Although TMDPDFs are defined from time-dependent light-cone correlations and

*Contact author: xgao@bnl.gov

Published by the American Physical Society under the terms of the Creative Commons Attribution 4.0 International license. Further distribution of this work must maintain attribution to the author(s) and the published article's title, journal citation, and DOI. Funded by SCOAP³.

inaccessible on a Euclidean lattice, they can be computed within the large-momentum effective theory framework [34–36] via the quasi-TMDPDFs [37–50]. At large hadron momentum, the quasi-TMDPDFs are matched to their light-cone counterparts through an effective theory expansion [40–42,47], enabling access to observables such as the Collins-Soper (CS) kernel for TMD evolution [51–60], soft function [55,56,58], and nucleon and pion TMDPDFs [61–64].

Traditional lattice calculations of quasi-TMDPDFs use nonlocal quark bilinears with staple-shaped Wilson lines, which introduce linearly power divergence and substantial statistical noise, especially at large b_T (or equivalently small k_T), thus limiting the precision. The recently developed Coulomb-gauge (CG) quasi-TMDPDF approach [65,66] addresses these issues by eliminating Wilson lines entirely, which not only reduces the statistical noise but also simplifies the renormalization. The CG method has enabled improved CS kernel calculations [67,68] and the first lattice determination of the pion TMDPDF with the soft function [69], demonstrating its potential for advancing TMD studies.

In this Letter, we present the first lattice QCD calculation of the isovector helicity and flavor-dependent unpolarized TMDPDFs in the proton, taking advantage of the CG method. The calculation employs chiral-symmetry-preserving domain-wall fermion discretization and physical quark masses, and reaches the nonperturbative region up to $b_T \approx 1$ fm, which corresponds to $k_T \sim 200$ MeV. By forming renormalization- and factorization-scale-independent ratios, we enable direct comparisons with phenomenological fits without requiring a separate determination of the soft function. Our results show a remarkable similarity between the isovector helicity and unpolarized TMDPDFs at moderate x, and reveal only mild flavor dependence in the unpolarized TMDPDFs—providing the first lattice benchmark in these channels. These findings offer valuable nonperturbative constraints for global analyses and establish a solid foundation for future lattice studies of the proton's 3D spin structure.

Theoretical framework—The bare CG quasi-TMD beam functions are defined as matrix elements of nonlocal quark bilinears with spatial separations in both the transverse (b_T) and longitudinal (b_z) directions, sandwiched between boosted hadron states,

$$\tilde{h}^B(b_T, b_z, P_z, \mu) = \langle \lambda; P_z | \mathcal{O}_\Gamma(b_T, b_z) | \lambda; P_z \rangle, \quad (1)$$

with $\mathcal{O}_\Gamma(b_T, b_z) = \bar{\psi}[b_T, (b_z/2)]\Gamma\psi[0, -(b_z/2)]|_{\nabla\cdot\mathbf{A}=0}$. Here, ψ is the quark field, $\nabla \cdot \mathbf{A} = 0$ is the CG condition, P_z is the hadron momentum, λ the hadron polarization, and Γ specifies the TMDPDF spin structure. This contrasts with the gauge-invariant (GI) quasi-TMD beam function, where nonlocal quark fields are connected by staple-shaped Wilson lines to preserve gauge invariance (see, e.g., Ref. [37]).

After appropriate renormalization of $\tilde{h}^B$—as explained below—and Fourier transform (FT) of the renormalized operator $\tilde{h}^R$ with respect to b_z, one obtains the quasi-TMD beam function $\tilde{f}(x, b_T, P_z, \mu)$, which is related to the light-cone TMDPDF $f(x, b_T, \zeta, \mu)$ via the factorization formula [40–42,47,66],

$$\frac{\tilde{f}(x, b_T, P_z, \mu)}{\sqrt{S_r(b_T, \mu)}} = H(xP_z, \mu) \exp\left[\frac{\gamma^{\overline{\rm MS}}(b_T, \mu)}{2} \ln \frac{(2xP_z)^2}{\zeta}\right] \times f(x, b_T, \zeta, \mu) + \mathcal{O}\left(\frac{\Lambda_{\rm QCD}}{xP_z}, \frac{1}{b_T(xP_z)}\right), \quad (2)$$

with power corrections suppressed by $1/(xP_z)$ [70], so that the factorization is valid in the moderate-x region but is expected to break down near the endpoints. Here, μ and ζ are the factorization and rapidity scales. The evolution in ζ is governed by the CS kernel $\gamma^{\overline{\rm MS}}(b_T, \mu)$ [3,71]. $H(xP_z, \mu)$ is a hard kernel obtained at one loop [66], and $S_r(b_T, \mu)$ is the intrinsic soft factor [41].

This factorization is independent of quark flavor and spin and does not involve gluon mixing [47]. These features enable the construction of renormalization-group-invariant (RGI) ratios from quasi-TMD beam functions that are free from scheme and scale dependence. In particular, the cancellation of the soft factor, hard kernel, and scale evolution terms makes the RGI ratios identical to their light-cone counterparts to all orders in perturbation theory, up to power-suppressed corrections.

For example, the ratio of proton isovector helicity TMDPDF $g_{1L}^{\Delta u_+ - \Delta d_+}$ to isovector unpolarized TMDPDF $f_1^{u_v - d_v}$ can be expressed as

$$R^{u-d}_{g_{1L}/f_1}(x, b_T) \cdot g_A \equiv \frac{g_{1L}^{\Delta u_+ - \Delta d_+}(x, b_T, \zeta, \mu)}{f_1^{u_v - d_v}(x, b_T, \zeta, \mu)} = \frac{\tilde{g}_{1L}^{\Delta u_+ - \Delta d_+}(x, b_T, P_z, \mu)}{\tilde{f}_1^{u_v - d_v}(x, b_T, P_z, \mu)}, \quad (3)$$

where g_A is the isovector axial charge of the proton and accounts for an overall normalization. Similarly, the RGI ratio of unpolarized up u- and down d-quark TMDPDFs of proton is

$$R^{u/d}_{f_1}(x, b_T) \equiv \frac{f_1^{u_v}(x, b_T, \zeta, \mu)}{f_1^{d_v}(x, b_T, \zeta, \mu)} = \frac{\tilde{f}_1^{u_v}(x, b_T, P_z, \mu)}{\tilde{f}_1^{d_v}(x, b_T, P_z, \mu)}. \quad (4)$$

Here, $q_v = q - \bar{q}$ corresponds to the valence quark contributions to the proton unpolarized TMDPDFs and $\Delta q_+ = \Delta q + \Delta\bar{q}$ represents the combined contribution of quarks and antiquarks to the proton helicity TMDPDF, where $q = u$ or d.

Lattice QCD calculations—The quasi-TMD beam function matrix elements are extracted from proton three-point correlation functions,

$$C^{\mathrm{3pt}}_{\mathcal{P},\Gamma}(t_s,\tau;b_T,b_z,P_z)=\sum_{\vec{y},\vec{x}}e^{-iP_z(y_z-x_z)}\mathcal{P}^{\mathrm{3pt}}_{\alpha\beta}\times\langle N_\alpha(\vec{y},t_s+t)\mathcal{O}_\Gamma\times(b_T,b_z,\tau+t)\bar{N}_\beta(\vec{x},t)\rangle. \quad (5)$$

We use the proton interpolating field $N^s_\alpha(\vec{x},t)=\varepsilon_{abc}u^s_{a\alpha}(\vec{x},t)[u^s_b(\vec{x},t)^T(\gamma_t\gamma_y)\gamma_5 d^s_c(\vec{x},t)]$, where the superscript s denotes smeared quark fields. The source position of N is denoted by $(\vec{x},t)$, t_s is the source-sink separation, τ is the operator insertion time, and $\mathcal{P}^{\mathrm{3pt}}_{\alpha\beta}$ selects the nucleon spin polarization. For the helicity case, we use $\Gamma=i\gamma_5\gamma_z$ and $\mathcal{P}^{\mathrm{3pt}}_{\alpha\beta}=\frac{1}{2}(1+\gamma_t)i\gamma_5\gamma_z$; for the unpolarized case, we use $\Gamma=\gamma_t$ and $\mathcal{P}^{\mathrm{3pt}}_{\alpha\beta}=\frac{1}{2}(1+\gamma_t)$.

The lattice calculations are performed using 81 gauge-field configurations of the $2+1$-flavor domain-wall fermion ensemble 64I [72], with five-dimensional volume $N_s^3\times N_t\times L_5=64^3\times 128\times 12$, physical up, down, and strange quark masses, and spacing $a=0.0836$ fm.

To improve ground-state overlap and reduce statistical noise, we employ boosted Gaussian smearing [73] of the quark fields in the interpolation operator. Gaussian smearing is implemented with radius $r_G=0.75$ fm and quark boost parameter $j_z=0$ and 3 [74,75], corresponding to nucleon momentum $P_z=2\pi n_z/(N_s a)$ with $n_z=0$ and 7, yielding $P_z^{\max}=1.62$ GeV.

Quark propagators are computed from CG-fixed gauge configurations using a deflated solver with 2000 eigenvectors. For each gauge configuration, we perform multiple measurements of $C^{\mathrm{3pt}}_{\mathcal{P},\Gamma}$ using the all-mode averaging technique [76]. For $n_z=0$, we compute one exact solve [77,78] (solver tolerance 10^{-8}) and four sloppy solves (solver tolerance 10^{-4}) at $t_s/a=\{6,8,10\}$. For $n_z=7$, we compute 1 exact and $\{16,32,64,128\}$ sloppy solves at $t_s/a=\{4,6,8,10\}$, respectively.

We compute isovector $(u-d)$ contributions for both helicity and unpolarized quasi-TMD beam functions. To study flavor dependence, the isoscalar $(u+d)$ channel is also calculated for the unpolarized case, neglecting quark-line disconnected contributions. These contributions are expected to be small [79–81], compared to the other systematic uncertainties. A dedicated investigation is needed in future work to quantify them.

Results—We extract the bare matrix elements of the CG quasi-TMD beam functions by analyzing the ratio of three-point to two-point correlators,

$$r(t_s,\tau;b_T,b_z,P_z)=\frac{C^{\mathrm{3pt}}(t_s,\tau;b_T,b_z,P_z)}{C^{\mathrm{2pt}}(t_s;P_z)}, \quad (6)$$

where C^{2pt} denotes the two-point correlator of the unpolarized proton. In the limit $\tau, t_s-\tau\to\infty$, the excited-state contributions are exponentially suppressed, and the ratio isolates the ground-state matrix elements $\tilde{h}^B(b_T,b_z,P_z,a)$. For finite t_s and τ, we apply three extraction strategies: one-state and plateau fit ($\mathrm{Fit}_{\mathrm{st1}}$), two-state fit ($\mathrm{Fit}_{\mathrm{st2}}$), and summation fit (SumFit).

In $\mathrm{Fit}_{\mathrm{st1}}$, we fit a constant to the stable region of r for $t_s=6a,8a,10a$, excluding up to $\tau=3a$ at both ends of each source-sink separation. For $\mathrm{Fit}_{\mathrm{st2}}$, we use $\tau\in[2a,t_s-2a]$ for joint fit of $t_s\in[4a,10a]$ and truncate the spectral sum in both C^{2pt} and C^{3pt} to include only the ground and first excited states. We extract the two energy levels and corresponding overlap amplitudes from fits to C^{2pt}, which are then used in the spectral decomposition of r to fit the matrix elements. For SumFit, we use r at $t_s=4a,6a,8a,10a$, summing over $\tau\in[2a,t_s-2a]$, and extract the matrix element from the slope of a linear fit in t_s. All fits are performed with an uncorrelated χ^2, with correlations preserved through configuration-wise bootstrap. More details can be found in Supplemental Material [82].

Figure 1 shows representative results at $P_z=1.62$ GeV, $b_T=8a$, and $b_z=0$, for the unpolarized and helicity matrix elements. The consistency across different methods indicates that excited-state effects are under control. For the final analysis, we average over all three methods on a

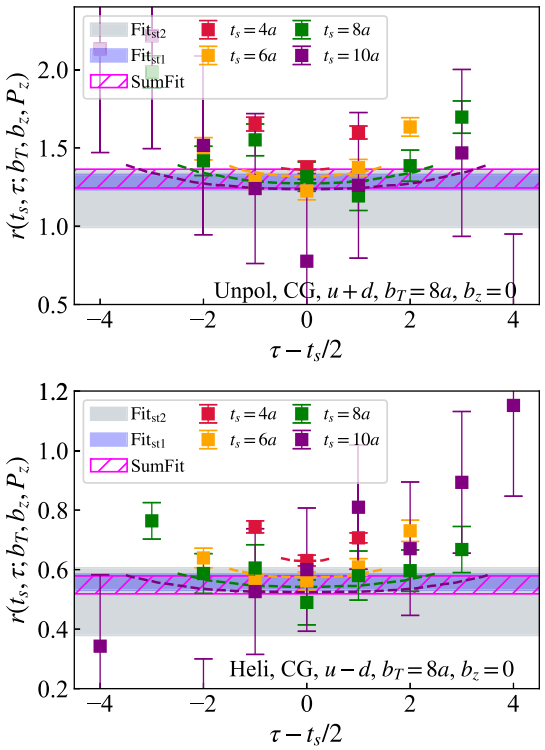

FIG. 1. Ratios $r(t_s,\tau;b_T,b_z,P_z=1.62\ \mathrm{GeV})$ for unpolarized (top) and helicity (bottom) CG quasi-TMD beam function matrix elements at $b_T=8a$ and $b_z=0$. Dashed lines show results from two-state fits; bands indicate the extracted values from $\mathrm{Fit}_{\mathrm{st1}}$, $\mathrm{Fit}_{\mathrm{st2}}$, and SumFit.

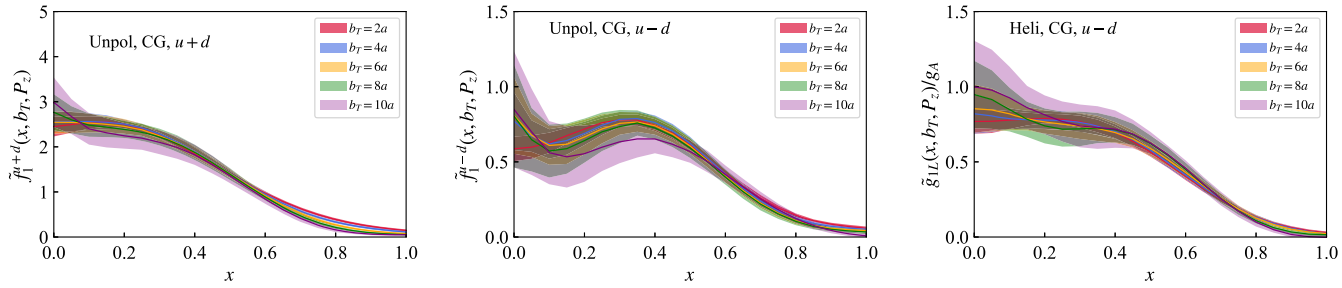

FIG. 2. The x-dependent quasi-TMD beam functions are presented as functions of x at several values of b_T. From left to right, the panels the isoscalar unpolarized, isovector unpolarized, and isovector helicity cases, respectively.

bootstrap sample-by-sample basis. Additional details and examples are provided in Supplemental Material [82].

The bare matrix elements require renormalization. For CG quasi-TMD beam functions, this reduces to a multiplicative constant independent of the quark separation $\{b_T, b_z\}$ and external hadron states [65,83]. Following Refs. [60,67], we apply the ratio

$$\tilde{h}_i^R(b_T, b_z, P_z) = \mathcal{N}\frac{\tilde{h}_i^B(b_T, b_z, P_z, a)}{\tilde{h}_{f_1}^{B,u_v-d_v}(b_T, 0, 0, a)}, \tag{7}$$

where the numerator corresponds to any operator or flavor channel considered in this Letter, and the denominator is fixed to the isovector unpolarized matrix element to cancel the common ultraviolet divergence [65]. $\mathcal{N} = \tilde{h}_{f_1}^{B,u_v-d_v}(0,0,0,a)/\tilde{h}_i^B(0,0,P_z,a)$ is a normalization factor. Although this renormalization depends on b_T, it cancels in the ratios of quasi-TMD beam functions, which we present as the final results. Nevertheless, its inclusion is useful for reducing common systematic errors in intermediate steps such as discretization artifacts and excited-state contamination. This Letter focuses exclusively on the real part of the matrix element, which provides access to the valence-quark contribution q_v in the unpolarized case and the combined quark-antiquark contribution Δq_+ in the helicity case. Previous studies [84–86] have shown that PDFs (or their even moments) extracted from the real part of the matrix elements agree well with global fits.

Due to confinement, the spatial correlators decay exponentially to zero at large b_z [87], making the FT numerically stable. To ensure smooth behavior and suppress the noise at large b_z, we apply an exponential extrapolation for $b_z \gtrsim 1$ fm [88]. The associated systematic uncertainty is estimated by varying the extrapolation range, which has negligible impact on the moderate-x region. After renormalization and FT, we obtain the helicity quasi-TMD beam function $\tilde{g}_{1L}^{\Delta u_+ - \Delta d_+}(x, b_T, P_z)$ and the unpolarized quasi-TMD beam functions $\tilde{f}_1^{u_v-d_v}(x, b_T, P_z)$ and $\tilde{f}_1^{u_v+d_v}(x, b_T, P_z)$, shown in Fig. 2 According to Eq. (2), the quasi-TMD beam function approximates the TMDPDF in x space at $\zeta = (2xP_z)^2$, up to a b_T-dependent normalization factor—the soft function—as well as matching and power corrections. Since the renormalization factor in Eq. (7) introduces b_T dependence, the renormalized quasi-TMD beam function is not monotonic in b_T. Nevertheless, we observe that it becomes increasingly suppressed as b_T grows when $x \to 1$, indicating that the $O(1/(xP_z b_T))$ power correction is suppressed, which is consistent with previous lattice findings [58,59,59,67,69]. The statistical errors of the quasi-TMD beam function decrease with increasing x and become small in the valence quark region. Although these errors grow with increasing b_T due to the worsening signal-to-noise ratio, they remain sufficiently controlled to allow for meaningful predictions. Next, we construct the RGI ratios of the quasi-TMD beam functions. As a cross-check, we also compute the gauge-invariant (GI) quasi-TMD beam functions using the same lattice setup, and confirm that their RGI ratios are consistent with those from the CG method, as expected from Eq. (2), [43,47,66]; see Supplemental Material [82].

Figure 3 shows the RGI ratio $R^{u-d}_{g_{1L}/f_1}(x, b_T)$, defined in Eq. (3), for several values of x. Across all x in the range [0.2, 0.6], the ratio is consistent with being constant in b_T within errors. This indicates that within the Collins-Soper-Sterman (CSS) [3] formalism of parametrizing the

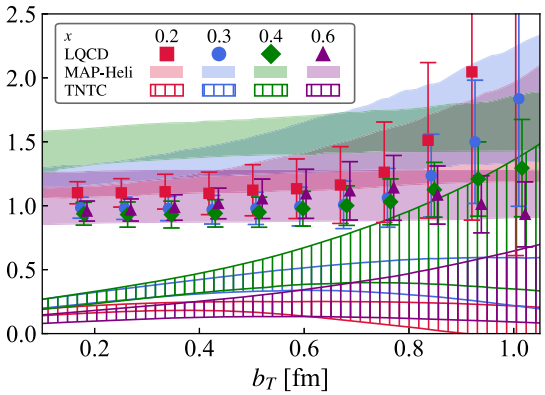

FIG. 3. Lattice QCD results (filled symbols with error bars) for the ratio $R^{u-d}_{g_{1L}/f_1}(x, b_T)$ of isovector helicity to isovector unpolarized TMDPDFs in Eq. (3), shown as a function of b_T at several values of x. The hatched bands indicate the corresponding global fits from MAP-Heli [33] and TNTC [32].

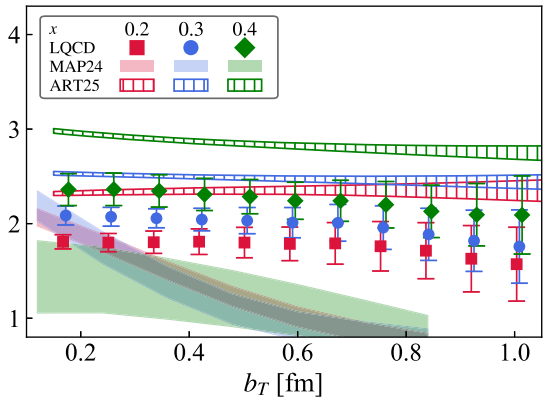

FIG. 4. Lattice QCD results (filled symbols with error bars) for the ratio $R_{f_1}^{u/d}(x, b_T)$ of up- to down-quark unpolarized TMDPDFs in Eq. (4), shown as a function of b_T at several values of x. The hatched bands denote the corresponding global fits from MAP24 [31] and ART25 [29].

TMDPDFs, the intrinsic nonperturbative TMD part is not sensitive to spin. At smaller x, particularly around $x = 0.2$, our results are consistent with the MAP-Heli fit [33], while some deviations emerge at larger x. However, the TNTC fit [32] yields substantially lower values across the entire x range, although its b_T dependence is also mild within uncertainties. The observed discrepancies between MAP-Heli and TNTC could be due to the experimental precision, analysis method, and model uncertainties. While our lattice calculation is performed at a single lattice spacing and momentum, and thus subject to discretization effects and power corrections, these effects have been shown to be under control in similar LaMET studies, such as the pion valence quark PDF [89], the CS kernel [67], and the proton unpolarized PDF [85]. Therefore, our lattice results in the moderate-x region can meaningfully differentiate and constrain phenomenological parameterizations of the TMDPDFs.

Figure 4 shows the ratio $R_{f_1}^{u/d}(x, b_T)$ of the valence u to d unpolarized TMDPDFs, as defined in Eq. (4), for several values of x. For comparison, results from the flavor-dependent global fits MAP24 [31] and ART25 [29] are shown as bands. Better agreement in the trends in b_T is observed between lattice and ART25, which also show a flat b_T dependence across all x. Nevertheless, the magnitudes of the two results are noticeably different, which is subject to their own systematic uncertainties. At small b_T, some similarity between the lattice results and MAP24 emerges, likely due to the dominance of input collinear PDFs in their analysis. The mild b_T variation in our lattice results indicates that the intrinsic nonperturbative TMD part of CSS parameterization has a weak dependence on the quark flavor. Notably, while the b_T dependence appears flat, the ratio still shows a noticeable dependence on x, indicating nontrivial longitudinal structure. Our finding is particularly valuable in light of the tensions among existing global fits, where incorporating flavor dependence introduces additional parameters that may increase statistical instability and contribute to systematic uncertainty. Therefore, our lattice QCD results offer a first-principles benchmark to guide future global analyses and help reduce the associated uncertainties.

Conclusion—We presented the first lattice QCD calculation of the isovector helicity TMDPDF and the flavor-dependent unpolarized TMDPDFs for up and down quarks in the proton. This calculation used domain wall fermion configurations with physical quark masses, and the CG method was employed to reliably access the deep nonperturbative region up to $b_T \sim 1$ fm.

We obtain ratios of the TMDPDFs, which can be directly compared to those from global analyses. Our results show a close similarity between the helicity and unpolarized isovector TMDPDFs at moderate x, as well as a mild flavor dependence in the unpolarized case. With the current precision, our results can differentiate phenomenological parameterizations of the TMDPDFs and be used as valuable inputs to constrain future global analyses.

The present study provides first benchmarks at moderate x on a single lattice spacing and volume, and neglects disconnected diagrams in the unpolarized channel. Future work will extend these results by increasing the proton momentum, employing finer lattices, and addressing additional systematics—including excited-state contamination, disconnected diagrams, and finite-volume effects—so as to reach precision-level control. In parallel, together with a lattice determination of the soft function [41,69], these improvements will enable precise predictions of the proton's three-dimensional structure with full spin dependence.

Acknowledgments—This material is based upon work supported by the U.S. Department of Energy, Office of Science, Office of Nuclear Physics through Contracts No. DE-SC0012704 and No. DE-AC02-06CH11357, and within the frameworks of Scientific Discovery through Advanced Computing (SciDAC) award Fundamental Nuclear Physics at the Exascale and Beyond and the Topical Collaboration in Nuclear Theory Quark Gluon Tomography (QGT) with Award DE-SC0023646. This research used awards of computer time provided by the INCITE program at Argonne Leadership Computing Facility, a DOE Office of Science User Facility operated under Contract DE-AC02-06CH11357; the ALCC program at the Oak Ridge Leadership Computing Facility, which is a DOE Office of Science User Facility supported under Contract DE-AC05-00OR22725; and the National Energy Research Scientific Computing Center, a DOE Office of Science User Facility supported by the Office of Science of the U.S. Department of Energy under Contract DE-AC02-05CH11231, using NERSC awards NP-ERCAP0028137 and NP-ERCAP0032114. Our calculations were performed using the Grid [90,91] and GPT [92] software packages.

We thank Christoph Lehner for his advice on using GPT. We thank the RBC and UKQCD collaborations for sharing the gauge field configurations used in our Letter.

Data availability—The data that support the findings of this Letter are openly available [1].

[1] J. Dudek *et al.*, Eur. Phys. J. A **48**, 187 (2012).
[2] A. Accardi *et al.*, Eur. Phys. J. A **60**, 173 (2024).
[3] J. C. Collins, D. E. Soper, and G. F. Sterman, Nucl. Phys. **B250**, 199 (1985).
[4] S. Amoroso *et al.*, Acta Phys. Pol. B **53**, 12 (2022).
[5] D. Boer *et al.*, arXiv:1108.1713.
[6] A. Accardi *et al.*, Eur. Phys. J. A **52**, 268 (2016).
[7] R. Abdul Khalek *et al.*, arXiv:2203.13199.
[8] R. Abir *et al.*, arXiv:2305.14572.
[9] C. T. H. Davies, B. R. Webber, and W. J. Stirling, Nucl. Phys. **B256**, 413 (1985).
[10] G. A. Ladinsky and C. P. Yuan, Phys. Rev. D **50**, R4239 (1994).
[11] F. Landry, R. Brock, P. M. Nadolsky, and C. P. Yuan, Phys. Rev. D **67**, 073016 (2003).
[12] A. V. Konychev and P. M. Nadolsky, Phys. Lett. B **633**, 710 (2006).
[13] P. Sun, J. Isaacson, C. P. Yuan, and F. Yuan, Int. J. Mod. Phys. A **33**, 1841006 (2018).
[14] U. D'Alesio, M. G. Echevarria, S. Melis, and I. Scimemi, J. High Energy Phys. 11 (2014) 098.
[15] A. Bacchetta, F. Delcarro, C. Pisano, M. Radici, and A. Signori, J. High Energy Phys. 06 (2017) 081; 06 (2019) 051(E).
[16] I. Scimemi and A. Vladimirov, Eur. Phys. J. C **78**, 89 (2018).
[17] V. Bertone, I. Scimemi, and A. Vladimirov, J. High Energy Phys. 06 (2019) 028.
[18] I. Scimemi and A. Vladimirov, J. High Energy Phys. 06 (2020) 137.
[19] A. Bacchetta, V. Bertone, C. Bissolotti, G. Bozzi, F. Delcarro, F. Piacenza, and M. Radici, J. High Energy Phys. 07 (2020) 117.
[20] F. Hautmann, I. Scimemi, and A. Vladimirov, Phys. Lett. B **806**, 135478 (2020).
[21] M. Bury, F. Hautmann, S. Leal-Gomez, I. Scimemi, A. Vladimirov, and P. Zurita, J. High Energy Phys. 10 (2022) 118.
[22] A. Bacchetta, V. Bertone, C. Bissolotti, G. Bozzi, M. Cerutti, F. Piacenza, M. Radici, and A. Signori (MAP (Multi-Dimensional Analyses of Partonic Distributions) Collaboration), J. High Energy Phys. 10 (2022) 127.
[23] J. Isaacson, Y. Fu, and C. P. Yuan, Phys. Rev. D **110**, 073002 (2024).
[24] F. Aslan, M. Boglione, J. O. Gonzalez-Hernandez, T. Rainaldi, T. C. Rogers, and A. Simonelli, Phys. Rev. D **110**, 074016 (2024).
[25] A. Vladimirov, J. High Energy Phys. 10 (2019) 090.
[26] M. Cerutti, L. Rossi, S. Venturini, A. Bacchetta, V. Bertone, C. Bissolotti, and M. Radici (MAP (Multi-Dimensional Analyses of Partonic Distributions) Collaboration), Phys. Rev. D **107**, 014014 (2023).
[27] P. C. Barry, L. Gamberg, W. Melnitchouk, E. Moffat, D. Pitonyak, A. Prokudin, and N. Sato (Jefferson Lab Angular Momentum (JAM) Collaboration), Phys. Rev. D **108**, L091504 (2023).
[28] A. Bacchetta, V. Bertone, C. Bissolotti, M. Cerutti, M. Radici, S. Rodini, and L. Rossi (MAP (Multi-Dimensional Analyses of Partonic Distributions) Collaboration), Phys. Rev. Lett. **135**, 021904 (2025).
[29] V. Moos, I. Scimemi, A. Vladimirov, and P. Zurita, arXiv:2503.11201.
[30] V. Moos, I. Scimemi, A. Vladimirov, and P. Zurita, J. High Energy Phys. 05 (2024) 036.
[31] A. Bacchetta, V. Bertone, C. Bissolotti, G. Bozzi, M. Cerutti, F. Delcarro, M. Radici, L. Rossi, and A. Signori (MAP Collaboration), J. High Energy Phys. 08 (2024) 232.
[32] K. Yang, T. Liu, P. Sun, Y. Zhao, and B.-Q. Ma, Phys. Rev. Lett. **134**, 121902 (2025).
[33] A. Bacchetta, A. Bongallino, M. Cerutti, M. Radici, and L. Rossi, Phys. Rev. Lett. **134**, 121901 (2025).
[34] X. Ji, Phys. Rev. Lett. **110**, 262002 (2013).
[35] X. Ji, Sci. China Phys. Mech. Astron. **57**, 1407 (2014).
[36] X. Ji, Y. Liu, Y. S. Liu, J.-H. Zhang, and Y. Zhao, Rev. Mod. Phys. **93**, 035005 (2021).
[37] X. Ji, P. Sun, X. Xiong, and F. Yuan, Phys. Rev. D **91**, 074009 (2015).
[38] X. Ji, L.-C. Jin, F. Yuan, J.-H. Zhang, and Y. Zhao, Phys. Rev. D **99**, 114006 (2019).
[39] M. A. Ebert, I. W. Stewart, and Y. Zhao, Phys. Rev. D **99**, 034505 (2019).
[40] M. A. Ebert, I. W. Stewart, and Y. Zhao, J. High Energy Phys. 09 (2019) 037.
[41] X. Ji, Y. Liu, and Y.-S. Liu, Nucl. Phys. **B955**, 115054 (2020).
[42] X. Ji, Y. Liu, and Y.-S. Liu, Phys. Lett. B **811**, 135946 (2020).
[43] M. A. Ebert, S. T. Schindler, I. W. Stewart, and Y. Zhao, J. High Energy Phys. 09 (2020) 099.
[44] A. A. Vladimirov and A. Schäfer, Phys. Rev. D **101**, 074517 (2020).
[45] X. Ji, Y. Liu, A. Schäfer, and F. Yuan, Phys. Rev. D **103**, 074005 (2021).
[46] X. Ji and Y. Liu, Phys. Rev. D **105**, 076014 (2022).
[47] M. A. Ebert, S. T. Schindler, I. W. Stewart, and Y. Zhao, J. High Energy Phys. 04 (2022) 178.
[48] S. T. Schindler, I. W. Stewart, and Y. Zhao, J. High Energy Phys. 08 (2022) 084.
[49] R. Zhu, Y. Ji, J.-H. Zhang, and S. Zhao, J. High Energy Phys. 02 (2023) 114.
[50] S. Rodini and A. Vladimirov, J. High Energy Phys. 09 (2023) 117.
[51] P. Shanahan, M. Wagman, and Y. Zhao, Phys. Rev. D **102**, 014511 (2020).
[52] P. Shanahan, M. Wagman, and Y. Zhao, Phys. Rev. D **104**, 114502 (2021).
[53] M. Schlemmer, A. Vladimirov, C. Zimmermann, M. Engelhardt, and A. Schäfer, J. High Energy Phys. 08 (2021) 004.
[54] H.-T. Shu, M. Schlemmer, T. Sizmann, A. Vladimirov, L. Walter, M. Engelhardt, A. Schäfer, and Y.-B. Yang, Phys. Rev. D **108**, 074519 (2023).

[55] Q.-A. Zhang *et al.* (Lattice Parton Collaboration), Phys. Rev. Lett. **125**, 192001 (2020).
[56] Y. Li *et al.*, Phys. Rev. Lett. **128**, 062002 (2022).
[57] M.-H. Chu *et al.* (LPC Collaboration), Phys. Rev. D **106**, 034509 (2022).
[58] M.-H. Chu *et al.* (Lattice Parton (LPC) Collaboration), J. High Energy Phys. 08 (2023) 172.
[59] A. Avkhadiev, P. E. Shanahan, M. L. Wagman, and Y. Zhao, Phys. Rev. D **108**, 114505 (2023).
[60] A. Avkhadiev, P. E. Shanahan, M. L. Wagman, and Y. Zhao, Phys. Rev. Lett. **132**, 231901 (2024).
[61] J.-C. He, M.-H. Chu, J. Hua, X. Ji, A. Schäfer, Y. Su, W. Wang, Y. Yang, J.-H. Zhang, and Q.-A. Zhang (LPC Collaboration), Phys. Rev. D **109**, 114513 (2024).
[62] M.-H. Chu *et al.*, Phys. Rev. D **109**, L091503 (2024).
[63] L. Walter *et al.*, Phys. Rev. D **111**, 094507 (2025).
[64] L. Ma *et al.* (LPC Collaboration), J. High Energy Phys. 08 (2025) 086.
[65] X. Gao, W.-Y. Liu, and Y. Zhao, Phys. Rev. D **109**, 094506 (2024).
[66] Y. Zhao, Phys. Rev. Lett. **133**, 241904 (2024).
[67] D. Bollweg, X. Gao, S. Mukherjee, and Y. Zhao, Phys. Lett. B **852**, 138617 (2024).
[68] S. Mukherjee, D. Bollweg, X. Gao, and Y. Zhao, Proc. Sci. DIS2024 (**2025**) 238 [arXiv:2407.10739].
[69] D. Bollweg, X. Gao, J. He, S. Mukherjee, and Y. Zhao, Phys. Rev. D **112**, 034501 (2025).
[70] Y. Liu and Y. Su, J. High Energy Phys. 02 (2024) 204.
[71] J. C. Collins and D. E. Soper, Nucl. Phys. **B193**, 381 (1981); **B213**, 545(E) (1983).
[72] T. Blum *et al.* (RBC, UKQCD Collaborations), Phys. Rev. D **108**, 054507 (2023).
[73] G. S. Bali, B. Lang, B. U. Musch, and A. Schäfer, Phys. Rev. D **93**, 094515 (2016).
[74] X. Gao, N. Karthik, S. Mukherjee, P. Petreczky, S. Syritsyn, and Y. Zhao, Phys. Rev. D **104**, 114515 (2021).
[75] X. Gao, L. Jin, C. Kallidonis, N. Karthik, S. Mukherjee, P. Petreczky, C. Shugert, S. Syritsyn, and Y. Zhao, Phys. Rev. D **102**, 094513 (2020).
[76] E. Shintani, R. Arthur, T. Blum, T. Izubuchi, C. Jung, and C. Lehner, Phys. Rev. D **91**, 114511 (2015).
[77] C. Aubin, T. Blum, C. Tu, M. Golterman, C. Jung, and S. Peris, Phys. Rev. D **101**, 014503 (2020).
[78] T. Blum, N. Christ, M. Hayakawa, T. Izubuchi, L. Jin, C. Jung, and C. Lehner, Phys. Rev. Lett. **118**, 022005 (2017).
[79] C. Alexandrou, M. Constantinou, K. Hadjiyiannakou, K. Jansen, and F. Manigrasso, Phys. Rev. D **104**, 054503 (2021).
[80] C. Alexandrou, S. Bacchio, M. Constantinou, J. Finkenrath, K. Hadjiyiannakou, K. Jansen, G. Koutsou, H. Panagopoulos, and G. Spanoudes, Phys. Rev. D **101**, 094513 (2020).
[81] J. Liang, M. Sun, Y.-B. Yang, T. Draper, and K.-F. Liu, Phys. Rev. D **102**, 034514 (2020).
[82] See Supplemental Material at http://link.aps.org/supplemental/10.1103/tb2w-3tks for more details of analysis and comparison between CG and GI approaches.
[83] K. Zhang, Y.-K. Huo, X. Ji, A. Schaefer, C.-J. Shi, P. Sun, W. Wang, Y.-B. Yang, and J.-H. Zhang (Lattice Parton Collaboration), Phys. Rev. D **110**, 074505 (2024).
[84] X. Gao, A. D. Hanlon, S. Mukherjee, P. Petreczky, Q. Shi, S. Syritsyn, and Y. Zhao, Phys. Rev. D **109**, 054506 (2024).
[85] X. Gao, A. D. Hanlon, J. Holligan, N. Karthik, S. Mukherjee, P. Petreczky, S. Syritsyn, and Y. Zhao, Phys. Rev. D **107**, 074509 (2023).
[86] Z. Fan, X. Gao, R. Li, H.-W. Lin, N. Karthik, S. Mukherjee, P. Petreczky, S. Syritsyn, Y.-B. Yang, and R. Zhang, Phys. Rev. D **102**, 074504 (2020).
[87] X. Gao, A. D. Hanlon, S. Mukherjee, P. Petreczky, P. Scior, S. Syritsyn, and Y. Zhao, Phys. Rev. Lett. **128**, 142003 (2022).
[88] X. Ji, Y. Liu, A. Schäfer, W. Wang, Y.-B. Yang, J.-H. Zhang, and Y. Zhao, Nucl. Phys. **B964**, 115311 (2021).
[89] X. Gao, A. D. Hanlon, N. Karthik, S. Mukherjee, P. Petreczky, P. Scior, S. Shi, S. Syritsyn, Y. Zhao, and K. Zhou, Phys. Rev. D **106**, 114510 (2022).
[90] P. A. Boyle, G. Cossu, A. Yamaguchi, and A. Portelli, Proc. Sci. LATTICE2015 (**2016**) 023.
[91] A. Yamaguchi, P. Boyle, G. Cossu, G. Filaci, C. Lehner, and A. Portelli, Proc. Sci. LATTICE2021 (**2022**) 035 [arXiv:2203.06777].
[92] C. Lehner *et al.*, Grid Python toolkit (GPT), https://github.com/lehner/gpt.